Mycobacterial fatty acid catabolism is repressed by FdmR to sustain lipogenesis and virulence

Wenyue Dong[a,b], Xiaoqun Nie[a], Hong Zhu[a], Qingyun Liu[c], Kunxiong Shi[d], Linlin You[a,b], Yu Zhang[a], Hongyan Fan[d], Bo Yan[d], Chen Niu[d,1], Liang-Dong Lyu[d,1], Guo-Ping Zhao[a,d,e], and Chen Yang[a,1]

[a]CAS Key Laboratory of Synthetic Biology, CAS Center for Excellence in Molecular Plant Sciences, Chinese Academy of Sciences (CAS), Shanghai 200032, China; [b]University of Chinese Academy of Sciences, Beijing 100049, China; [c]Department of Immunology and Infectious Diseases, Harvard T. H. Chan School of Public Health, Boston, MA 02115; [d]Key Laboratory of Medical Molecular Virology of the Ministry of Education/National Health Commission/Chinese Academy of Medical Sciences (MOE/NHC/CAMS), School of Basic Medical Sciences, Department of Microbiology, School of Life Sciences, Shanghai Public Health Clinical Center, Fudan University, Shanghai 200000, China; and [e]Bio-Med Big Data Center, CAS Key Laboratory of Computational Biology, Shanghai Institute of Nutrition and Health, Chinese Academy of Sciences, Shanghai 200032, China

Edited by Dirk Schnappinger, Weill Cornell Medicine, New York, NY, and accepted by Editorial Board Member Carl F. Nathan March 3, 2021 (received for review September 13, 2020)

Host-derived fatty acids are an important carbon source for pathogenic mycobacteria during infection. How mycobacterial cells regulate the catabolism of fatty acids to serve the pathogenicity, however, remains unknown. Here, we identified a TetR-family transcriptional factor, FdmR, as the key regulator of fatty acid catabolism in the pathogen *Mycobacterium marinum* by combining use of transcriptomics, chromatin immunoprecipitation followed by sequencing, dynamic ^{13}C-based flux analysis, metabolomics, and lipidomics. An *M. marinum* mutant deficient in FdmR was severely attenuated in zebrafish larvae and adult zebrafish. The mutant showed defective growth but high substrate consumption on fatty acids. FdmR was identified as a long-chain acyl-coenzyme A (acyl-CoA)–responsive repressor of genes involved in fatty acid degradation and modification. We demonstrated that FdmR functions as a valve to direct the flux of exogenously derived fatty acids away from β-oxidation toward lipid biosynthesis, thereby avoiding the overactive catabolism and accumulation of biologically toxic intermediates. Moreover, we found that FdmR suppresses degradation of long-chain acyl-CoAs endogenously synthesized through the type I fatty acid synthase. By modulating the supply of long-chain acyl-CoAs for lipogenesis, FdmR controls the abundance and chain length of virulence-associated lipids and mycolates and plays an important role in the impermeability of the cell envelope. These results reveal that despite the fact that host-derived fatty acids are used as an important carbon source, overactive catabolism of fatty acids is detrimental to mycobacterial cell growth and pathogenicity. This study thus presents FdmR as a potentially attractive target for chemotherapy.

Mycobacterium | fatty acid | metabolic regulation | lipid homeostasis

In the 1950s, it was determined that *Mycobacterium tuberculosis*, the causative agent of human tuberculosis, preferentially metabolizes fatty acids when recovered from the lungs of infected animals (1). Since then, numerous studies have demonstrated that pathogenic mycobacteria scavenge fatty acids and cholesterol from hosts and utilize them as primary sources of carbon and energy during infection (2–7). Multiple genes involved in fatty acid and cholesterol catabolism have been shown to be essential for mycobacterial growth and survival in various infection models (8–12).

Fatty acids are metabolized to meet the catabolic and anabolic needs of mycobacterial cells after conversion to their acyl-coenzyme A (acyl-CoA) derivatives (13, 14). Degradation of fatty acids through β-oxidation can provide energy and building blocks for biomass synthesis. With each turn of the β-oxidation cycle, the fatty acyl-CoA loses a two-carbon fragment as acetyl-CoA, which is further metabolized through the tricarboxylic acid (TCA) cycle and the glyoxylate shunt. Another product, propionyl-CoA, which can be generated through β-oxidation of odd-chain fatty acids or degradation of branched-chain amino acids and cholesterol, enters the methylmalonyl-CoA pathway and the methylcitrate cycle (15–17). Acetyl-CoA is used as a primer for de novo synthesis of long-chain fatty acids through the multifunctional type I fatty acid synthase (FAS-I) (18). Long-chain fatty acids are biosynthetic precursors for production of the virulence-associated polyketide lipids by polyketide synthases and for synthesis of the mycolic acids through elongation with the specialized fatty acid synthase II (FAS-II) complex (19, 20). Fatty acids are also incorporated directly into cell membrane phospholipids or stored as triacylglycerol.

Multiple use of fatty acids places a premium on regulatory mechanisms to ensure a balance between fatty acid degradation and lipid anabolism. The fatty acid degradation in many bacteria is thus controlled in response to the availability of fatty acids to maintain lipid homeostasis. For example, a GntR-family transcriptional regulator, FadR, represses the β-oxidation genes in *Escherichia coli* in the absence of an exogenous source of fatty acids, and this repression is antagonized by long-chain acyl-CoAs (21, 22). Mycobacterial cells utilize transcriptional factors MabR and FadR as regulators of an operon for FAS-II and FasR as a regulator of the gene encoding FAS-I, and the activity of these three regulators is modulated by long-chain acyl-CoAs (23–25). However, the regulatory mechanisms that control the fatty acid catabolism in mycobacteria remain largely to be elucidated. Although a few global transcriptional regulators, including the dormancy survival regulator DosR, the

Significance

An improved understanding of fatty acid metabolism in pathogenic mycobacteria is critical for development of new chemotherapeutics. Here, we identified FdmR, a previously uncharacterized transcriptional factor, as the key regulator of fatty acid catabolism in the pathogen *Mycobacterium marinum*. We demonstrated that FdmR optimizes fatty acid utilization and allows for a high rate of cell growth with modest consumption of the nutrients. Moreover, we found that FdmR suppresses degradation of de novo-synthesized fatty acids and controls the size and abundance of virulence-associated lipids and mycolates. These results reveal that FdmR-mediated regulation serves important functions in mycobacterial physiology and pathogenicity. Thus, this study identifies FdmR as a potentially attractive target for novel therapeutic intervention.

Author contributions: C.N., L.-D.L., G.-P.Z., and C.Y. designed research; W.D., X.N., H.Z., Q.L., K.S., L.Y., and H.F. performed research; Y.Z. contributed new reagents/analytic tools; W.D., X.N., B.Y., C.N., L.-D.L., and C.Y. analyzed data; and W.D., X.N., and C.Y. wrote the paper.

The authors declare no competing interest.

This article is a PNAS Direct Submission. D.S. is a guest editor invited by the Editorial Board.

[1]To whom correspondence may be addressed. Email: chniu@fudan.edu.cn, liangdong.lv@gmail.com, or cyang@cemps.ac.cn.

This article contains supporting information online at https://www.pnas.org/lookup/suppl/doi:10.1073/pnas.2019305118/-/DCSupplemental.

Published April 14, 2021.

hypoxia response regulator Rv0081, and the cholesterol catabolic regulator KstR, have been found to regulate genes involved in fatty acid degradation in *M. tuberculosis* (26–28), none of them are essentially responsive to the availability of fatty acids. Understanding of how mycobacterial cells regulate their fatty acid catabolism to serve the pathogenicity can lead to discovery of novel targets for antimycobacterial chemotherapy (29).

In this study, we identified a TetR-like transcriptional factor that regulates genes of fatty acid degradation and modification in *Mycobacterium marinum*, which is a fish, amphibian, and opportunistic human pathogen (30). *M. marinum*–infected zebrafish are used as a model system for studying mycobacterial pathogenesis (31–33), and *M. marinum* also utilizes host-derived fatty acids as an important carbon source during infection (6). The regulator, which we named FdmR, was encoded by *MMAR_0500* and *rv0238* in *M. marinum* and *M. tuberculosis*, respectively. Inactivation of *rv0238* seems to be of no consequence in *M. tuberculosis*, as shown by screening of a transposon mutant library (8, 34), whereas recent studies have identified *rv0238* as one of the genes required for *M. tuberculosis* infection in mice (35, 36). The function of Rv0238 and its orthologs in mycobacteria remains unknown. Here, the crucial role of FdmR in *M. marinum* virulence was revealed through infection in zebrafish larvae and adult zebrafish. We determined the FdmR regulon by combining transcriptomic analysis with chromatin immunoprecipitation followed by sequencing (ChIP-Seq). The metabolic signal perceived by FdmR was identified as long-chain acyl-CoAs. However, the seemingly contradictory phenotypes were observed for the mutant deficient in FdmR, which exhibited relatively high substrate consumption but impaired cell growth on fatty acids. Then, we combined dynamic ^{13}C-based flux analysis, metabolomics, and lipidomics to study the regulatory function of FdmR. Our results led to the conclusion that FdmR acts as a key player in optimization of fatty acid utilization and regulation of lipid homeostasis in mycobacterial cells.

Results

FdmR Is Crucial for *M. marinum* Virulence. To assess the role of FdmR in mycobacterial virulence, we generated a gene deletion mutant, Δ*fdmR*, of *M. marinum* and a genetically complemented counterpart, Δ*fdmR*/C (*SI Appendix*, Fig. S1). The virulence of the *M. marinum* strains was evaluated using the zebrafish infection model. Adult zebrafish were infected at a high dosage (~5,000 colony-forming units [CFU]) and their survival was monitored over a 3-wk time course. Fish infected with the wild-type or complemented strains exhibited high mortality (end-point mortality >67%), whereas an increased survival (end-point mortality ~17%) was observed for fish infected with the Δ*fdmR* mutant (Fig. 1*A*). Histological analysis of fish infected with the wild-type or complemented strains showed granuloma formation associated with a large number of bacteria at 1 wk postinfection (wpi) and more granulomas with necrotic areas accompanied by patches of bacteria outside of granulomas at 3 wpi (Fig. 1*B*). By contrast, when fish were infected with the Δ*fdmR* mutant, no granuloma was detectable at 1 wpi, and organized granulomas were formed at 3 wpi, but with little evidence of necrosis and few bacteria detected outside granulomas. The replication of the *M. marinum* strains was examined in zebrafish larvae, which lack functional lymphocytes (37). Larvae were infected with about 100 CFU of the *M. marinum* strains and the bacterial burden was examined at 3 d and 6 d postinfection (dpi). Compare to the wild type, the Δ*fdmR* mutant was found to be severely attenuated in larvae (Fig. 1 *C* and *D*). Moreover, the growth of the Δ*fdmR* mutant in macrophages was markedly impaired compared with that of the wild type (*SI Appendix*, Fig. S2). Complementation of the Δ*fdmR* strain restored the growth in macrophages. Together, these findings demonstrate that FdmR is crucial for *M. marinum* virulence, which prompted us to perform comprehensive characterization of the FdmR regulon.

FdmR Represses Genes of Fatty Acid Degradation and Modification. To understand how FdmR may affect gene expression, we performed a comparative transcriptomic analysis for the Δ*fdmR* mutant versus the wild type using RNA sequencing (RNA-Seq). A total of 80 genes were differentially expressed between the two strains, of which 53 genes were up-regulated and 27 genes were down-regulated in the Δ*fdmR* mutant compared to the wild type (*SI Appendix*, Table S1). Among the most highly differentially expressed genes, we observed a considerable up-regulation of the genes (*fadA2*, *fadE12_3*, *fadE23-fadE24*, *echA8_7*, *echA10_1*, *desA3*, *acrA1*, and *fabG4-htdX*) involved in fatty acid metabolism in the Δ*fdmR* mutant (Fig. 2*A*). To further characterize the FdmR regulon, we employed ChIP-Seq to identify the genomic binding regions for FdmR (Fig. 2*B* and *SI Appendix*, Fig. S3). FdmR was found to bind upstream of *fadA2*, *fabG4*, *fadE24*, *fixA*, and *MMAR_1683*, which is consistent with the reported ChIP-Seq data for Rv0238 (38). New binding sites of FdmR were detected in the upstream regions of *fadE5*, *icl*, *desA3*, *desA3_1*, and *MMAR_2730* (Fig. 2*B* and *SI Appendix*, Fig. S3). Based on all the sequences enriched in the ChIP-Seq analysis, the conserved binding motif for FdmR was generated, which is comprised of the AT-rich inverted repeats (Fig. 2*C*). Fluorescence polarization assays (FPAs) verified that FdmR bound to all the target DNA operators directly and specifically (*SI Appendix*, Fig. S4*A*). The apparent dissociation constant (K_d) values of FdmR–DNA interactions varied from 15 nM to 77 nM, indicating different affinities of FdmR to different DNA operators. Thus, by combining use of RNA-Seq, ChIP-Seq, and FPAs, the FdmR regulon was determined, which includes *fadA2*, *fadE23-fadE24*, *MMAR_2729-MMAR_2730*, *fixA-fixB*, *fadE5*, *icl*, *desA3*, *desA3_1*, *fabG4-htdX*, and *MMAR_1683*. The *fadA2* and *fadE23-fadE24* encode enzymes of fatty acid β-oxidation (FAO) (18). The *fixA-fixB* gene products probably participate in FAO-related electron transport (39). The *fadE5* is likely involved in β-oxidation of the acyl side chain of cholesterol (40), and a recent study showed broad specificity of FadE5 for acyl-CoAs (41). The *icl* encodes multifunctional isocitrate lyase/methylisocitrate lyase required for both the glyoxylate shunt and the methylcitrate cycle (15, 42). The *desA3* and *desA3_1* encode acyl-CoA desaturases (18, 43), and *fabG4-htdX* has been proposed to be involved in fatty acid modification (44). Therefore, FdmR is a repressor of the genes mostly involved in fatty acid degradation and modification.

To identify the metabolic signal perceived by FdmR, we used FPAs to investigate the effects of various metabolites on the interaction between FdmR and its DNA operators. The intermediate metabolites associated with fatty acid degradation were tested, which include a long-chain fatty acid (oleate) and various acyl-CoAs with carbon chain length from C2 to C18. Addition of long-chain acyl-CoAs (C14 to C18) resulted in a decrease in the formation of FdmR–DNA complex in a concentration-dependent manner (Fig. 2*D* and *SI Appendix*, Fig. S4*B*), whereas no significant effect was observed for the same concentrations of oleate and acyl-CoAs with shorter chains (C2 to C12). Furthermore, we studied the effects of supplementation of fatty acids to cultures on expression of genes in the FdmR regulon. qRT-PCR analysis verified that all the 14 genes were up-regulated in the Δ*fdmR* mutant compared with the wild type when grown in the absence of fatty acids (Fig. 2*E*). Supplementation of long-chain fatty acids (a mixture of C16:0 palmitate, C18:0 stearate, and C18:1 oleate) to the wild-type culture significantly increased the transcript levels of most of the FdmR target genes except *fadE23-fadE24* and *desA3-desA3_1*. No increase in expression of *desA3-desA3_1* resulted from the presence of unsaturated fatty acid (oleate) in the medium, because up-regulation of *desA3-desA3_1* was observed when only palmitate and stearate were added to the wild-type culture (*SI Appendix*, Fig. S5*A*). Another approach to increasing intracellular long-chain acyl-CoA levels is the addition of inhibitors of the FAS-II complex, such as isoniazid (23, 45). We found that addition of isoniazid to the

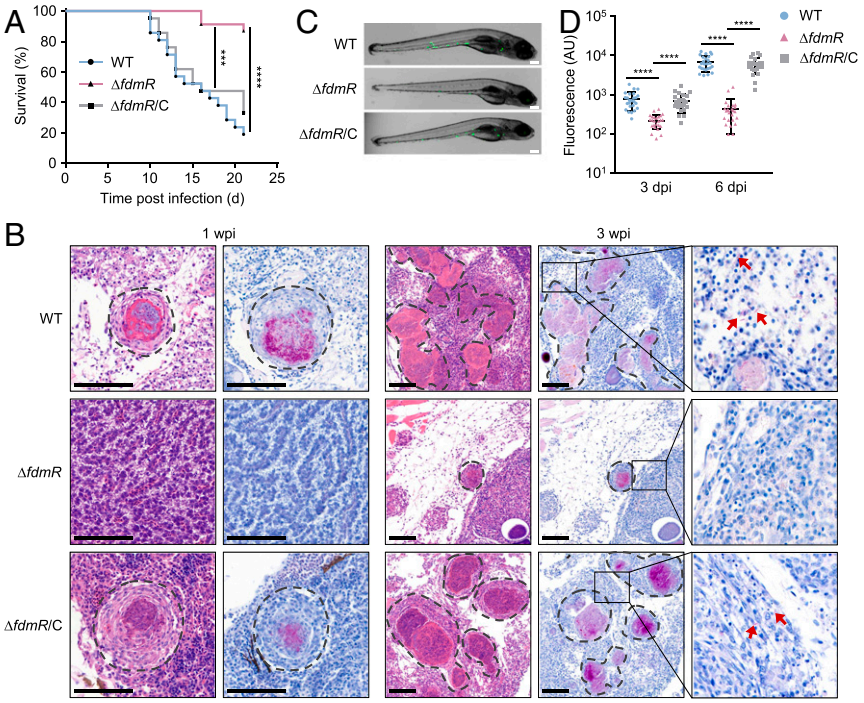

Fig. 1. FdmR is crucial for *M. marinum* virulence. (*A*) Survival of adult zebrafish infected with *M. marinum* wild type (WT), Δ*fdmR* mutant, and complemented strain Δ*fdmR*/C. $n = 25$ per group. ***$P < 0.001$, ****$P < 0.0001$ by Kaplan–Meier method with a log-rank test. (*B*) Hematoxylin–eosin (*Left*) and Ziehl–Neelsen (*Right*) stains of adult zebrafish at 1 wpi and 3 wpi. (Scale bars, 100 μm.) Dotted lines delineate granulomas. The boxed areas are enlarged on the right and arrows indicate bacteria outside granulomas. Results are representative of three experiments. (*C*) Representative images of zebrafish larvae infected with the *M. marinum* strains carrying a fluorescent protein-expressing plasmid at 6 dpi. (Scale bars, 200 μm.) (*D*) Bacterial burdens of zebrafish larvae at 3 dpi and 6 dpi. $n = 25$ per group. ****$P < 0.0001$ by unpaired two-tailed *t* test.

wild-type culture significantly up-regulated all of the FdmR target genes (*SI Appendix*, Fig. S5*B*). However, when a short-chain (C5:0 valerate) or a medium-chain (C10:0 decanoate) fatty acid was added to the wild-type culture no significant changes in expression levels of the FdmR target genes were observed (*SI Appendix*, Fig. S5*C*). In contrast to the wild type, the Δ*fdmR* mutant exhibited constitutively high expression of the FdmR target genes, regardless of the presence or absence of long-chain fatty acids in the culture (Fig. 2*E*). In addition, we did not observe significant differences between the two strains in expression of the TCA cycle genes and the canonical FadA/FadB β-oxidation complex–encoding genes, which are not members of the FdmR regulon (*SI Appendix*, Fig. S5*D*). Together, these results indicate that FdmR regulates its target genes in response to intracellular long-chain acyl-CoA levels.

We observed that the target genes of FdmR were differentially regulated. When long-chain fatty acids or isoniazid were added to the cultures, the expression levels of several target genes, including the FAO-associated genes *fadE23-fadE24* and *fadA2*, were significantly lower in the wild type than those in the Δ*fdmR* mutant (Fig. 2*E* and *SI Appendix*, Fig. S5*B*), which indicates the strong repression of these genes by FdmR. In contrast, the other genes such as *icl* showed similar expression levels in both strains grown with long-chain fatty acids. Moreover, we found that the inhibitory effect of long-chain acyl-CoAs on the interactions between FdmR and various DNA operators was different (Fig. 2*F*). In the presence of a high level of oleoyl-CoA (e.g., 5 μM) (46), FdmR completely dissociated from the *icl* operator, whereas a significant fraction of FdmR still bound to the *fadE24* and *fadA2* operators. These results suggested that the fatty acid catabolic genes regulated by FdmR are controlled in a hierarchical manner that depends on the intracellular concentrations of its ligand, long-chain acyl-CoAs.

FdmR Is Required for Optimal Growth on Fatty Acids. Due to the strong repression of FAO genes by FdmR, we asked if loss of FdmR would result in enhanced growth of mycobacterial cells on fatty acids and related substrates. To test it, we compared the growth between *M. marinum* wild type and the Δ*fdmR* mutant on carbon-defined minimal medium with various carbon sources. Both strains grew indistinguishably with glucose and glycerol (Fig. 3*A*). Unexpectedly, the Δ*fdmR* mutant showed a growth defect on oleate, acetate, and propionate as the sole carbon source. This growth defect could be fully complemented by expression of *fdmR* in the Δ*fdmR* strain. Supplementation of glucose and glycerol to the medium was unable to relieve the growth impairment of the Δ*fdmR* strain with fatty acids (*SI Appendix*, Fig. S6*A*). We found that compared with the wild type the growth rate of the Δ*fdmR* mutant decreased by 30 to 55% with fatty acid (oleate, palmitate, valerate, propionate, or acetate) as a carbon source (*SI Appendix*, Fig. S6*B*). Therefore, FdmR is required for optimal growth on fatty acids. This is consistent with our finding that FdmR is crucial for growth of *M. marinum* in macrophages and zebrafish. Meanwhile, we measured the oleate consumption during growth of the *M. marinum* strains (*SI Appendix*, Fig. S6*C*). Increased rates of oleate consumption were observed for the Δ*fdmR* mutant compared to the wild type (Fig. 3*B*), which was probably due to the up-regulation of FAO genes in the mutant. Thus, the seemingly contradictory results were obtained for the Δ*fdmR* strain that exhibited relatively high substrate consumption but impaired cell growth on fatty acids. Next, we sought to address this question by performing a systematic and quantitative analysis of the FdmR-mediated regulation of the fatty acid metabolism in *M. marinum*.

FdmR Deficiency Results in Overactive Catabolism of Fatty Acids. To quantify the flux through the fatty acid catabolic pathway, we

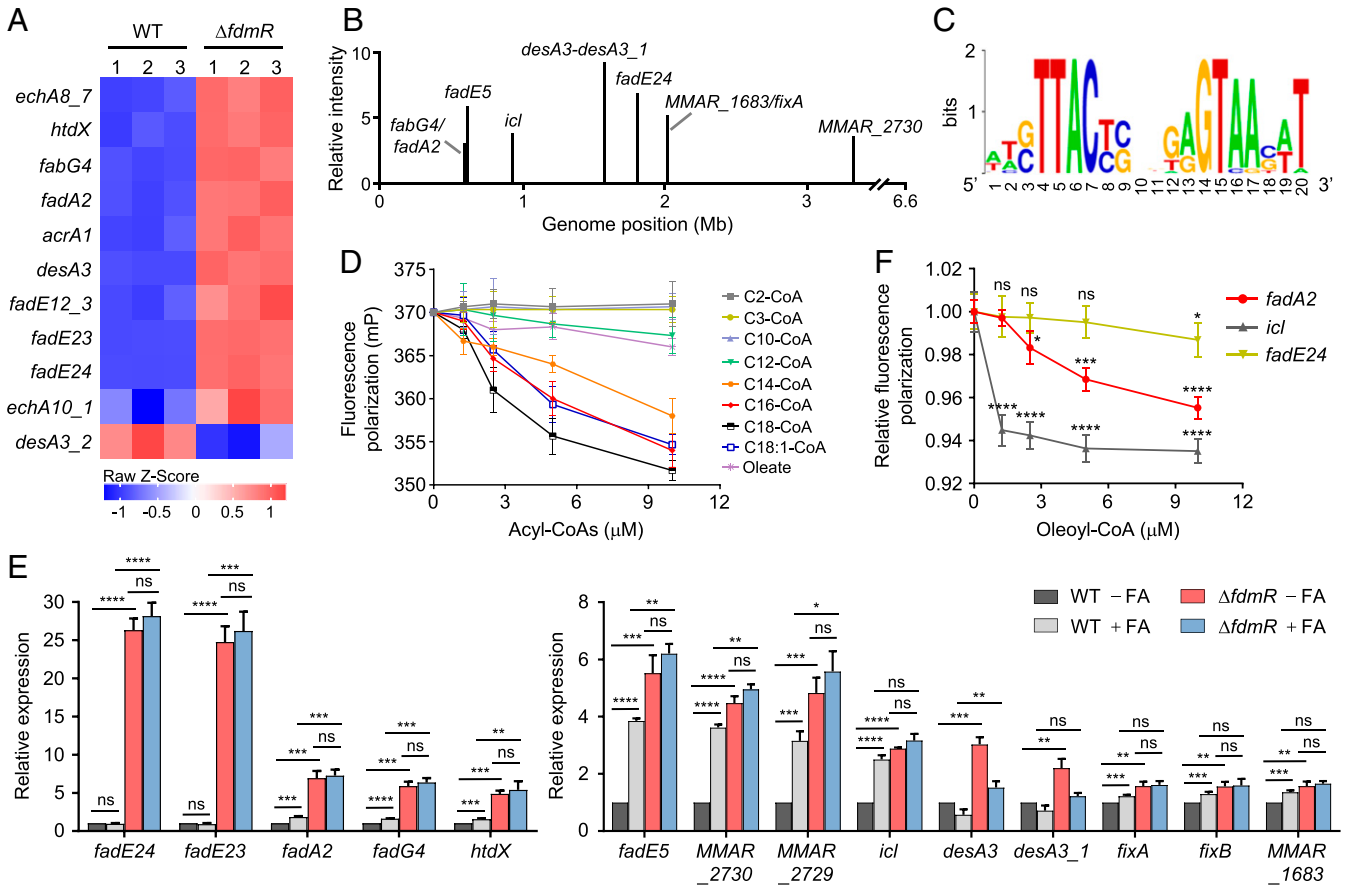

Fig. 2. Identification of FdmR regulon and effector molecules. (*A*) Heat map showing relative expression levels of the genes involved in fatty acid metabolism in *M. marinum*. The strains were grown in 7H9 medium with glycerol and OADC enrichment. Data shown are from three independent experiments. (*B*) Genome-wide FdmR-binding sites identified by ChIP-Seq. (*C*) Sequence logo of the FdmR-binding motif derived from ChIP-Seq enriched sequences. (*D*) Effect of various acyl-CoAs and oleate on the FdmR-DNA interaction determined by FPAs. The DNA operator of *fadA2* was used. (*E*) Effect of long-chain fatty acid supplementation on expression of FdmR target genes in wild type and Δ*fdmR* mutant. The strains were grown in 7H9 with glycerol and glucose. Long-chain fatty acids were added to the medium as indicated. The expression levels of each gene were determined by qRT-PCR and normalized to the gene expression in the wild type grown in the absence of fatty acids. (*F*) Effect of oleoyl-CoA on the interaction of FdmR with various DNA operators. Data are normalized to the value in the absence of oleoyl-CoA. Data shown in *D*, *E*, and *F* are mean ± SD ($n = 3$ independent experiments). *$P < 0.05$, **$P < 0.01$, ***$P < 0.001$, ****$P < 0.0001$, not significant (ns), by unpaired two-tailed *t* test with false discovery rate correction.

conducted dynamic ^{13}C labeling experiments on filter cultures by using uniformly labeled (*U*) [*U*-^{13}C]oleate, [*U*-^{13}C]acetate, or [*U*-^{13}C]propionate as tracers. We switched growing mycobacterial cultures from unlabeled to labeled fatty acid by using a filter perfusion method (47). The dynamic labeling of individual metabolites was then analyzed through rapid and frequent sampling followed by liquid chromatography–mass spectrometry (LC-MS) and gas chromatography–MS (GC-MS) measurements (*SI Appendix*, Fig.

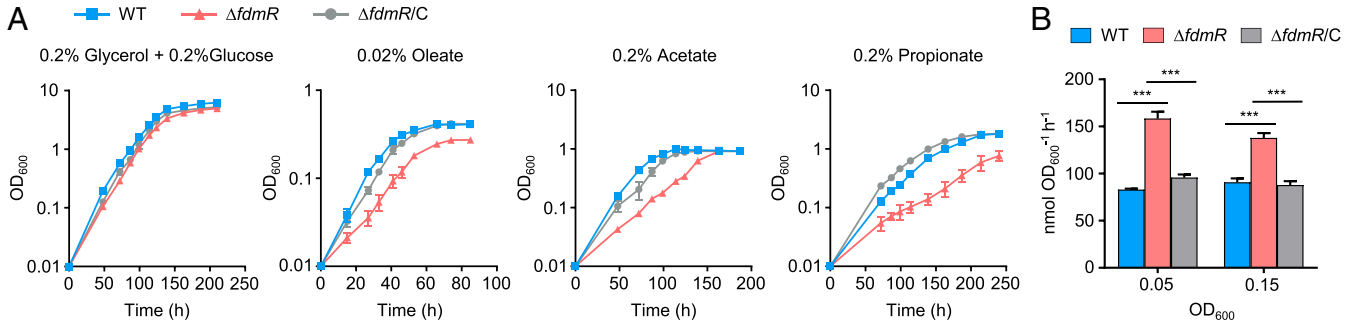

Fig. 3. FdmR deficiency results in impaired growth and increased substrate consumption of *M. marinum* on fatty acids. (*A*) Growth of *M. marinum* wild type, Δ*fdmR* mutant, and complemented strain Δ*fdmR*/C in modified Sauton's medium supplemented with glycerol and glucose, oleate, acetate, or propionate as the only carbon source. (*B*) Oleate consumption rate per OD_{600}. Data shown are mean ± SD ($n = 3$ independent experiments). ***$P < 0.001$, by unpaired two-tailed *t* test.

S7). During the switch to [*U*-^{13}C]oleate, intracellular oleoyl-CoA and acetyl-CoA were substantially labeled within 5 s (Fig. 4*A*), and their dynamic labeling data allowed us to quantify the oleate-consumption flux and the FAO flux. The metabolic flux distribution through central carbon metabolism (CCM) was also determined based on the labeling data of the intermediate metabolites (*SI Appendix*, Fig. S7). In the wild type grown on oleate, 16% of oleoyl-CoA molecules converted from oleate were degraded through the FAO pathway and 84% were used for lipid synthesis (Fig. 4*B*). Of the acetyl-CoA molecules generated by FAO, 25% directly entered the glyoxylate shunt, and 25% were converted to isocitrate and further metabolized by the glyoxylate shunt. The remaining 50% were routed through the TCA cycle. Compared with the wild type, the Δ*fdmR* mutant exhibited a 1.5-fold increase in the oleate-consumption flux and a 2.3-fold increase in the FAO flux. The fluxes through both the glyoxylate shunt and the TCA cycle increased 2.3-fold in the Δ*fdmR* strain (Fig. 4*B*). During growth on acetate, an increased flux through the glyoxylate shunt was observed for the Δ*fdmR* mutant compared to the wild type (Fig. 4*C*). During growth on propionate, the Δ*fdmR* mutant showed higher fluxes through the methylcitrate cycle and the methylmalonyl-CoA pathway than the wild type (Fig. 4*D*).

To obtain a global view of the metabolic consequence of FdmR deficiency, we compared intracellular and extracellular metabolomes between the wild type and Δ*fdmR* mutant. A large number of intracellular metabolites of CCM were accumulated in the Δ*fdmR* mutant grown on oleate, acetate, or propionate (Fig. 4*E* and *SI Appendix*, Fig. S8*A*). Some of these metabolites are chemically reactive or biologically toxic intermediates. Glyoxylate toxicity has been reported for *M. tuberculosis* (48). 2-Methylcitrate, citrate, and malate are strong inhibitors of fructose 1,6-bisphosphatase that is required for bacterial growth on fatty acids (49, 50). Accumulation of chemically reactive intermediates such as fumarate or propionyl-CoA has been shown to result in an intoxication in *M. tuberculosis* (51, 52). Dihydroxyacetone phosphate (DHAP) and γ-aminobutyric acid (GABA) levels markedly increased in the Δ*fdmR* mutant compared with the wild type (Fig. 4*E*), which can lead to production of the highly reactive aldehyde methylglyoxal and growth-inhibitory succinate semialdehyde, respectively (53, 54). Accumulation of the ketones acetoacetate and β-hydroxybutyrate was observed in the Δ*fdmR* mutant grown on oleate and acetate, which was suggestive of ketoacidosis arising from the increased flux of acetyl-CoA synthesis. Exo-metabolomics analysis showed remarkable increases in extracellular levels of CCM intermediates including succinate, fumarate, malate, and aconitate for the Δ*fdmR* mutant compared with the wild type (*SI Appendix*, Fig. S8*B*), which indicates the overflow CCM owing to the increased FAO flux. The presence of these metabolites in the culture medium may inhibit secretion and enhance the intracellular accumulation of them (51, 55). In addition, we observed that intracellular acyl-CoAs with chain length from C4 to C14 were accumulated in the Δ*fdmR* mutant grown on oleate (Fig. 4*E*). Moreover, the levels of these short- or medium-chain acyl-CoAs also markedly increased in glycerol-, acetate-, or propionate-grown cells of the Δ*fdmR* mutant compared with the wild type (Fig. 4*E* and *SI Appendix*, Fig. S8*A*), in which long-chain acyl-CoAs were synthesized de novo through FAS-I. Together, these findings indicate that FdmR deficiency results in overactive catabolism of fatty acids from either an exogenous source or the endogenous biosynthesis. We speculate that the resulting changes in acyl-CoA profiles may lead to modified lipid anabolism, because acyl-CoAs serve as the precursors for lipid production.

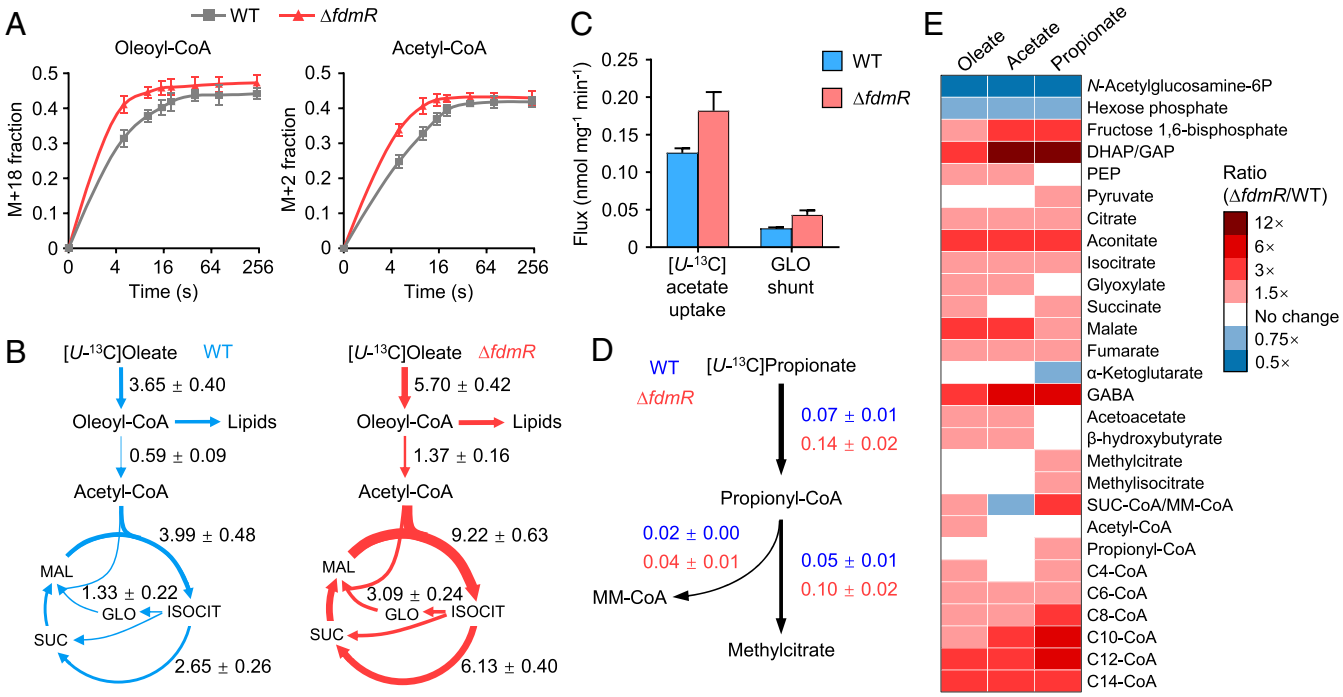

Fig. 4. FdmR deficiency results in overactive catabolism of fatty acids. (*A*) Kinetics of labeling of oleoyl-CoA and acetyl-CoA after switching *M. marinum* cells to [*U*-^{13}C]oleate medium. Data shown are mean ± SD ($n = 3$ independent experiments). (*B*) In vivo fluxes in fatty acid catabolism in *M. marinum* wild type and Δ*fdmR* mutant. ISOCIT, isocitrate; GLO, glyoxylate; SUC, succinate; MAL, malate. (*C*) In vivo fluxes of acetate assimilation and glyoxylate shunt in wild type and Δ*fdmR* mutant. (*D*) In vivo fluxes through methylmalonyl-CoA (MM-CoA) pathway and methylcitrate cycle in wild type and Δ*fdmR* mutant. The strains were grown on medium containing[*U*-^{13}C]oleate (*B*), [*U*-^{13}C]acetate (*C*), or [*U*-^{13}C]propionate (*D*). Data shown in *B*, *C*, and *D* are median ± 95% confidence interval ($n = 3$ independent experiments) and are expressed in nanomoles per milligram cell dry weight per minute. (*E*) Heat map showing the ratio of metabolite concentrations in the Δ*fdmR* mutant versus wild type during growth on oleate, acetate, or propionate. Data are means of three independent experiments and normalized to the values in the wild type.

FdmR Deficiency Results in Synthesis of Shortened Lipids. To test whether FdmR deficiency influences biosynthesis of fatty acids, we determined the ^{13}C labeling of fatty acids in the wild-type and Δ*fdmR* cells from stationary [*U*-^{13}C]acetate labeling experiments. Compared with the wild type, the Δ*fdmR* mutant showed notable increases in ^{13}C-labeled fatty acids with chain length of C10 and C12, which were derived mainly from degradation of endogenously synthesized long-chain fatty acids (Fig. 5*A*). In contrast, the ^{13}C-labeled fractions of fatty acids of C18 or longer were significantly reduced in the Δ*fdmR* mutant, indicating the decreased biosynthetic flux of these long-chain fatty acids in the mutant. Similar changes in the ^{13}C labeling patterns of fatty acids were observed in the Δ*fdmR* and wild-type cells from [*U*-^{13}C]oleate labeling experiments (*SI Appendix*, Fig. S9).

We studied the effect of FdmR deficiency on fatty acid composition of total lipids. The fatty acids were released from the extracted lipids by saponification and analyzed by GC-MS. The Δ*fdmR* mutant, compared with the wild type, exhibited markedly increased levels of fatty acids with length shorter than C18 and decreased levels of fatty acids longer than C18 when grown on oleate or acetate (Fig. 5*B*). Moreover, accumulation of fatty acids shorter than C17 and depletion of fatty acids of C17 or longer were observed for the Δ*fdmR* strain grown on propionate. In addition, the ratios of oleic acid (C18:1Δ9) to stearic acid (C18:0) and palmitoleic acid (C16:1Δ9) to palmitic acid (C16:0) were significantly higher in the acetate- or propionate-grown Δ*fdmR* mutant than the wild type (*SI Appendix*, Fig. S10), which was in accordance with up-regulation of *desA3* and *desA3_1* in the mutant.

We then compared the lipidome between the wild-type and Δ*fdmR* strains during growth in the presence of oleate (*SI Appendix*, Fig. S11). The amounts of phenolic glycolipid (PGL) and trehalose monomycolate (TMM) decreased by over 40% in the Δ*fdmR* mutant (Fig. 5*C*). A substantial reduction of trehalose dimycolate (TDM) was also observed for the mutant (*SI Appendix*, Fig. S12). PGL is a virulence-associated polyketide lipid in slow-growing mycobacteria including hypervirulent *M. tuberculosis* strains and displays immunosuppressive properties (56). TMM and TDM form the outer lipid barrier of mycobacterial cell envelop and serve as potent triggers of host inflammation (20, 57). Compared with the wild type, the Δ*fdmR* mutant also showed a significantly increased content of the storage molecule triacylglycerol (TAG), which could be due to a stress response (58), and altered levels of phospholipids (Fig. 5*C*). Moreover, for all the lipids detected, including PGL, phthiocerol dimycocerosate, TAG, diacylglycerol (DAG), phospholipids, TMMs, and free mycolates

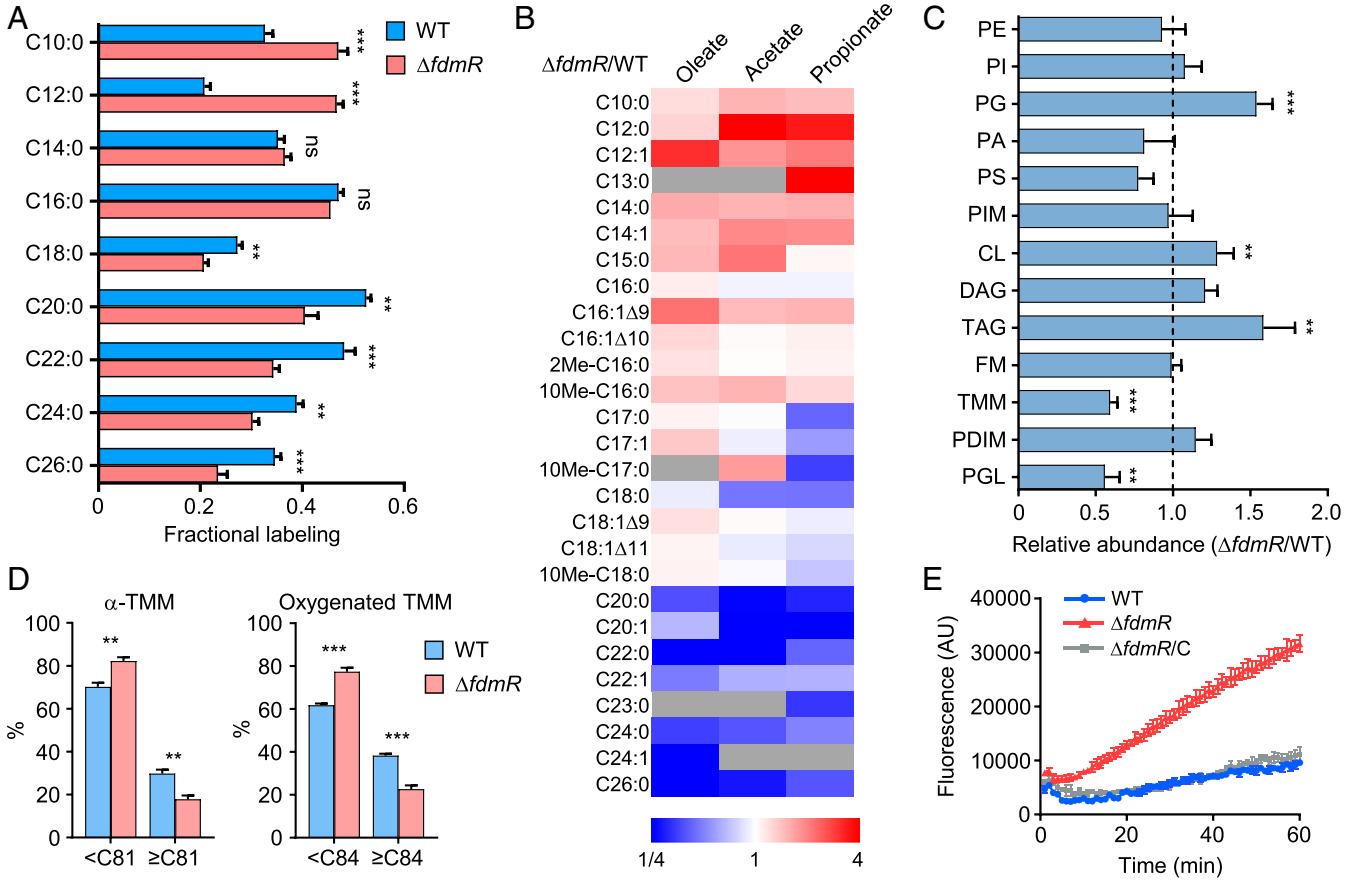

Fig. 5. FdmR deficiency results in synthesis of shortened lipids and increased cell-wall permeability. (*A*) ^{13}C fractional labeling of fatty acids in *M. marinum* wild type and Δ*fdmR* mutant grown on [*U*-^{13}C]acetate. (*B*) Ratio of fatty acid contents in the Δ*fdmR* mutant versus wild type during growth on oleate, acetate, or propionate. Gray color indicates that fatty acid is below detection limits. Data are means of three independent experiments, normalized to the values in the wild type. (*C*) Relative abundance of major lipids in *M. marinum* Δ*fdmR* mutant compared to the wild type. The strains were grown in 7H9 with glycerol and OADC. Abbreviations of phospholipids: PE, phosphatidylethanolamine; PI, phosphatidylinositol; PG, phosphatidylglycerol; PA, phosphatidic acid; PS, phosphatidylserine; PIM, phosphatidylinositol mannoside; CL, cardiolipin. (*D*) Fractions of relatively short and long species within α-TMM and oxygenated TMM in the wild type and Δ*fdmR* mutant. (*E*) Effect of FdmR deficiency on *M. marinum* cell-wall permeability determined by ethidium bromide accumulation assay. Data shown in *A, C, D,* and *E* are mean ± SD ($n = 3$ independent experiments). $^{**}P < 0.01$, $^{***}P < 0.001$, not significant (ns), by unpaired two-tailed *t* test.

(FMs), the alkane chain lengths were reduced in the Δ*fdmR* strain (Fig. 5*D* and *SI Appendix*, Fig. S11*B*). The fractions of relatively short species within each lipid class significantly increased, whereas the fractions of long species decreased in the Δ*fdmR* mutant compared to wild type. Thus, FdmR deficiency resulted in decreased levels of virulence-associated PGL, TMM, and TDM and synthesis of shortened mycolates and other lipids. These changes in lipid composition of mycobacterial cell wall could cause a defect in resisting host defense mechanisms (59).

Given the importance of mycolates in the impermeability of mycobacterial cell walls, we examined the cell-wall permeability using the ethidium bromide accumulation assay and the antibiotic susceptibility of the *M. marinum* strains. The Δ*fdmR* mutant showed a much higher accumulation rate of ethidium bromide than the wild type (Fig. 5*E*), which indicates the increased permeability of the mutant's cell wall. Moreover, the Δ*fdmR* mutant was more susceptible than the wild type to rifampicin, erythromycin, and ciprofloxacin, with 8- to 16-fold lower minimal inhibitory concentration (MIC) (*SI Appendix*, Table S2). Relatively small (two- to fourfold) differences were detected for the two strains in resistance to isoniazid, ethambutol, and streptomycin. Complementation of the Δ*fdmR* strain by expressing *fdmR* fully restored the cell-wall impermeability and resistance to the antibiotics (Fig. 5*E* and *SI Appendix*, Table S2). Thus, FdmR deficiency resulted in a defect in the permeability barrier of mycobacterial cell wall.

Discussion

While fatty acids have long been recognized as an important carbon source for pathogenic mycobacteria during infection, it remains unknown how mycobacterial cells regulate the catabolism in response to the availability of fatty acids from hosts. In this study, we identified FdmR, a TetR-family transcriptional factor, as the key regulator of fatty acid catabolism in *M. marinum*. The mutant deficient in FdmR showed defective growth on fatty acids and severe attenuation in zebrafish. Through a combination of transcriptomic analysis with ChIP-Seq, FdmR was identified as a repressor of the FAO and CCM genes, which are differentially regulated by FdmR in response to long-chain acyl-CoA levels. By combining use of dynamic ^{13}C-based flux analysis, metabolomics, and lipidomics we demonstrated that the strong repression of FAO genes by FdmR avoids the overactive catabolism of fatty acids and accumulation of toxic CCM intermediates (*SI Appendix*, Fig. S13). Moreover, FdmR-mediated regulation enables sufficient supply of long-chain fatty acids for production of lipids with their full chain lengths. Thus, FdmR is a key player in optimization of fatty acid utilization, which acts as a valve to direct the fatty acid flux away from β-oxidation toward lipid biosynthesis. This control mechanism enables mycobacterial cells to grow at a high rate with modest consumption of fatty acid nutrients, which is strikingly different compared with the regulatory mechanisms used by other bacteria such as *E. coli* to support maximal utilization and degradation of fatty acids from the growth medium (21). The high growth efficiency on fatty acids may confer a growth advantage for pathogenic mycobacteria, which often reside in niches with restrictive nutrients (29). Our results thus reveal that inhibition of fatty acid catabolism is crucial for mycobacterial cell growth and pathogenicity. Therefore, FdmR is a potentially attractive target for chemotherapeutic intervention.

In mycobacteria, the long-chain acyl-CoAs synthesized by FAS-I are used as the precursors for production of lipids. Our study, however, indicates that the FAS-I–derived acyl-CoAs can be degraded through FAO (*SI Appendix*, Fig. S13). Fatty acid cycling through biosynthetic and degradative pathways, which constitute a waste of energy and assimilated carbon, is generally thought to be absent in bacteria. This is partly due to the fact that most bacteria lack FAS-I but utilize FAS-II for de novo fatty acid synthesis, which generates long-chain acyl-acyl carrier protein (ACP) (60). As mycobacterial cells possess exceptionally complex pathways of fatty acid metabolism, tight control of fatty acid fluxes between these pathways is essential to meet the need for synthesis of lipids. We found that degradation of the FAS-I–synthesized long-chain acyl-CoAs is generally suppressed by FdmR (*SI Appendix*, Fig. S13). However, when lipid synthesis is impaired (e.g., inhibition of the FAS-II complex by isoniazid), substantial accumulation of intracellular long-chain acyl-CoAs leads to derepression of FdmR target genes for the recycling of acyl-CoAs. FdmR-mediated regulation also supports the synthesis of longer-chain FAS-I products (Fig. 5*A* and *SI Appendix*, Fig. S9). FdmR deficiency resulted in production of shortened lipids and reduction of PGL, TMM, and TDM levels, which could be due to the decreased availability of longer-chain acyl-CoAs for synthesis of polyketide lipids and mycolates (61). Thus, by modulating the supply of long-chain acyl-CoAs for lipogenesis, FdmR controls the abundance and chain length of virulence-associated lipids and mycolates. Hence, besides the previously reported regulators of lipid anabolism (e.g., MabR and FasR) (14), FdmR is also a key modulator of lipid homeostasis. In particular, the FdmR-deficient mutant produced shorter mycolates and exhibited increased cell-wall permeability, which is similar to *M. tuberculosis* mutants of *kasB* encoding 3-oxoacyl-ACP synthase 2 of FAS-II (62, 63). Therefore, regulation of fatty acid catabolism is required for maintaining lipid homeostasis and impermeability of the mycobacterial cell envelope.

FdmR is widely present among mycobacteria. Notably, highly conserved homologs of FdmR (>78% sequence identity) were identified in many strict or opportunistic pathogens of mycobacteria, including members of the *M. tuberculosis* complex, *Mycobacterium leprae*, and nontuberculous mycobacteria (64) (*SI Appendix*, Fig. S14*A*). In contrast, FdmR protein is absent in animals, yeast, and most bacteria, although a relatively distant homolog is present in some species of *Corynebacteriales*. The FdmR regulons in mycobacterial species, which were reconstructed by a comparative genomic approach, are almost identical (*SI Appendix*, Fig. S14*B* and Table S3). According to the reconstructed regulons, the candidate target genes of FdmR in *M. tuberculosis* are likely the same as those in *M. marinum* except for the duplicate *desA3* gene present in the latter species. However, it remains unclear whether FdmR is important for *M. tuberculosis* virulence. Inconsistent results from screening of transposon mutant libraries have been reported on the essentiality of Rv0238 for *M. tuberculosis* infection in mice (8, 35, 36). Transcriptional profiling showed up-regulation of FdmR and down-regulation of almost all of its regulon genes in *M. tuberculosis* in infected macrophages isolated directly from mouse lungs (65), which suggests repression of fatty acid catabolism by FdmR during in vivo infection of *M. tuberculosis*. Further studies are needed to clarify the role of FdmR and characterize its regulatory function in *M. tuberculosis*. Finally, the genetic variation of FdmR in the whole-genome sequences of 10,220 clinical strains of *M. tuberculosis* was analyzed (66). Only 37 nucleotide substitutions of FdmR were found, including 11 nonsynonymous and 26 synonymous changes (*SI Appendix*, Table S4). The ratio of nonsynonymous and synonymous substitutions of FdmR was 0.18, which was much lower than those of the essential genes (median, 0.53) and nonessential genes (median, 0.65) (67), indicating that FdmR is under strong purifying selection.

Materials and Methods

Strains and Culture Conditions. *M. marinum* ATCC BAA-535 (strain M) and its derivative strains were routinely grown at 30 °C in Middlebrook 7H9 broth or on 7H10 agar supplemented with 0.4% glycerol, 10% oleic acid–albumin–dextrose–catalase (OADC; 0.6, 50, 20, and 0.03 g·L^{-1}, respectively), and 0.04% tyloxapol (broth only). For carbon-use experiments, strains were cultivated in carbon-defined minimal medium, which consisted of modified Sauton's medium (51, 68) supplemented with 0.2% glucose and 0.2% glycerol, 0.02% sodium oleate (with 1% fatty acid-free bovine serum albumin [BSA]), 0.2%

acetate, or 0.2% propionate as the sole carbon source. Strains were also grown in 7H9 with 0.5% BSA, 0.2% glucose, and 0.2% glycerol and supplemented with 0.0056% palmitate, 0.009% oleate, 0.2% acetate, 0.2% valerate, or 0.2% propionate as an additional carbon source. For growth curves, *M. marinum* cells were precultured to an optical density at 600 nm (OD_{600}) of ∼1.0, washed, and resuspended in fresh medium to an OD_{600} of ∼0.01. The cultures were grown at 30 °C in 100-mL shake flasks with 30 mL of media and OD_{600} measurements were made at successive time points. For metabolomic profiling, *M. marinum* cells were grown in modified Sauton's medium with 0.009% oleate or in 7H9 with 0.2% of acetate or propionate to an OD_{600} of ∼0.5. Because of the presence of citrate and glutamate in commercial 7H9 medium and the poor solubility of oleate, the modified Sauton's medium was used, in which oleate was the sole carbon source. For RNA-Seq and lipidomic profiling, *M. marinum* cells were grown in 7H9 with 0.2% glycerol and 10% OADC to an OD_{600} of ∼0.8. For transcriptional analysis using qRT-PCR, *M. marinum* cells were exponentially growing in 7H9 with 0.2% glucose, 0.2% glycerol, 1.5% fatty acid-free BSA, and 0.085% NaCl. Long-chain fatty acids (a mixture of 0.003% palmitate, 0.003% oleate, and 0.003% stearate), decanoate (0.01%), or valerate (0.05%) was added to the culture medium. Isoniazid (200 $\mu g \cdot mL^{-1}$) was added to exponentially growing cultures and cells were collected after 2-h treatment.

Mutant Construction and Complementation. The *fdmR* (*MMAR_0500*)-deficient mutant of *M. marinum* was constructed by replacing the target gene with the kanamycin resistance cassette as described previously (12). For complementation of Δ*fdmR*, the coding region along with the 300-bp upstream promoter region of the *fdmR* gene was cloned to pMV306 vector (12) and the resulting plasmid was integrated into the genome of Δ*fdmR* mutant. The complete list of strains and primers used in this study is shown in *SI Appendix*, Tables S5 and S6, respectively.

Zebrafish Infections. Zebrafish larvae were injected via the caudal vein with about 100 CFU of *M. marinum* strains carrying the Wasabi fluorescent protein-expressing vector pTEC15 (31) as described previously (69). Bacterial burdens in larvae were determined by fluorescence pixel counts using the EVOS FL color imaging system (Invitrogen) and ImageJ software. Adult zebrafish were infected by intraperitoneal injection with 10 μL of single-cell bacterial suspensions at a dosage of 5,000 CFU per fish (69). For survival experiments, 25 fish per group were infected with each of the *M. marinum* strains. For the histopathological study, three fish were killed at 1 and 3 wpi. Fish were fixed in 10% formalin, dehydrated with ethanol, and embedded in paraffin (69). Serial paraffin sections (5-μm thickness) were stained with a hematoxylin–eosin solution or with Ziehl–Neelsen staining. Sections were scanned by Pannoramic MIDI (3DHISTECH), and images were collected with CaseViewer software. Experimental protocols involving zebrafish were approved by the Institutional Animal Care and Use Committee of Fudan University (approval number 20160225-018).

Macrophage Infection. RAW 264.7 macrophages were infected with *M. marinum* strains and intracellular bacterial growth was measured as described previously (69).

Cell-Wall Permeability Assay. Cell-wall permeability of *M. marinum* strains was assayed by measuring the intracellular accumulation of ethidium bromide as previously reported (70). Cells exponentially growing in 7H9 with glycerol and OADC were washed and resuspended in potassium phosphate buffer (pH 7) to an OD_{600} of ∼0.4. After addition of ethidium bromide (2 μM), the fluorescence was monitored over time using a plate reader (Spark; Tecan) equipped with an excitation filter of 540/25 nm and an emission filter of 580/20 nm.

Antibiotic Susceptibility Assay. Susceptibility of *M. marinum* strains to antibiotics was determined in 7H9 with glycerol and OADC as previously described (69). The MIC was defined as the minimal concentration at which no visible growth occurred after 7 d of incubation.

Transcriptional Profiling. Total RNA isolation and sample preparation for RNA-Seq were performed as previously reported (71). RNA-Seq was conducted using the Illumina HiSeq 4000 system. Sequence reads were mapped to the *M. marinum* M strain reference sequence (GenBank GCA_000018345.1). Differential expression analysis for RNA-Seq was performed using edgeR (72). For a subset of genes, Z-score normalization was applied to their expression values that had been log-transformed. The qRT-PCR experiments were conducted with the *sigA* gene as an internal standard (71).

ChIP-Seq. To generate an *M. marinum* strain overexpressing C-terminal 3×FLAG-tagged FdmR protein, the *fdmR* gene along with the sequence encoding the 3×FLAG was cloned into pMV261 vector (73) and the resulting plasmid was transformed into the wild type. Cells were grown in 7H9 medium with 0.2% glycerol and 10% ADC to an OD_{600} of ∼0.8 and then cross-linked with 1% formaldehyde for 15 min at room temperature followed by quenching with 125 mM glycine. Sample preparation for ChIP-Seq was performed as previously reported (71) and purified DNA was sequenced in an Illumina NovaSeq 6000 by SeqHealth Tech. The MACS2 program (74) was employed for peak calling and the data were visualized using ggplot2 package. DNA sequences of enriched regions were subjected to a binding motif search with MEME (75).

Fluorescence Polarization Assay. For expression and purification of FdmR protein, the *M. marinum fdmR* gene was cloned into the vector pET28a and the resulting plasmid was used to produce the N-terminal hexahistidine-tagged FdmR. The 28- to 29-bp Cy5 fluorescence-labeled double-strand DNA fragments containing the upstream promoter regions of individual genes from *M. marinum* were chemically synthesized by Sangon Biotech. The DNA fragments (5 nM) were incubated at room temperature for 10 min with purified FdmR protein. FPAs were performed using a plate reader (Spark; Tecan) equipped with an excitation filter of 635/35 nm and an emission filter of 665/8 nm.

Dynamic Isotope Labeling Experiments. The labeling compounds including uniformly ^{13}C-labeled sodium oleate ([*U*-^{13}C]oleate), uniformly ^{13}C-labeled propionate ([*U*-^{13}C]propionate), and uniformly ^{13}C-labeled acetate ([*U*-^{13}C]acetate) were ≥99% pure and were purchased from Cambridge Isotope Lab. Dynamic isotope labeling experiments were performed using a variant of the filter cultivation method as previously reported (47). Briefly, *M. marinum* cells were grown in shake flasks with modified Sauton's medium supplemented with 0.09 $g \cdot L^{-1}$ oleate or in 7H9 with 1 $g \cdot L^{-1}$ of acetate or propionate to an OD_{600} of ∼0.3. Fifty-milliliter aliquots of the culture were transferred onto a nitrocellulose filter (0.45-μm pore size; Millipore) mounted on a vacuum device. Subsequently, cells were continuously perfused with the media containing 0.09 $g \cdot L^{-1}$ of a mixture of 50% (wt/wt) [*U*-^{13}C]oleate and 50% unlabeled oleate, or 1 $g \cdot L^{-1}$ of [*U*-^{13}C]propionate or [*U*-^{13}C]acetate. At various time points after isotope switch the filter was extracted after filtration and cell extracts were used for metabolite analysis. The stationary [*U*-^{13}C]acetate and [*U*-^{13}C]oleate labeling experiments were performed as reported previously (76), and the exponentially growing cells were collected for fatty acid analysis.

Metabolomics. Metabolism was quenched, and metabolites were extracted with −80 °C 80% methanol (77). Cells were lysed with 0.1-mm zirconia beads (Biospec) in a tissue homogenizer (Bertin) for 3 min at 6,500 rpm. The samples were centrifuged, and the supernatant was collected.

Cell extracts were analyzed by ultrahigh-performance liquid chromatograph (UHPLC; Acquity; Waters) coupled to a Q Exactive hybrid quadrupole-orbitrap mass spectrometer (Thermo Fisher). The injection volume was 10 μL. Metabolites were separated with a Luna NH2 column (100 mm × 2 mm, 3-μm particle size; Phenomenex) as described previously (78). The mass spectrometer was run in both electrospray ionization positive (ESI^+) and negative (ESI^-) modes. Data were acquired using full scan over 70 to 1,000 *m/z* at 70,000 resolution. MS/MS spectra were acquired with 30-eV collision energy. This method was used to generate data on most of the central metabolites, amino acids, and nucleotides. The compound identities were verified by mass and retention-time match to authenticated standards. Relative concentrations of metabolites were determined by using a calibration curve generated with varying concentrations of chemical standard spiked into mycobacterial cell extract.

Glyoxylate, pyruvate, isocitrate, citrate, methylcitrate, and methylisocitrate were analyzed by GC-MS (GC7890−MS7200QTOF; Agilent). The dried cell extracts were oximated with 20 $g \cdot L^{-1}$ methoxyamine hydrochloride in pyridine at 30 °C for 60 min and then derivatized with *N*-methyl-*N*-[*tert*-butyldimethylsilyl] trifluoroacetamide (Sigma) at 70 °C for 30 min. After filtration, 1 μL of samples were injected into the GC-MS system with an DB-5HT column (30 × 0.25 mm, 0.1 μm). The mass spectrometer was operated in the electron impact (EI) mode at 70 eV. This method enables good separation of the isomers isocitrate and citrate as well as methylcitrate and methylisocitrate.

Acyl-CoAs were analyzed by the above-mentioned UHPLC-MS system using a modified procedure (79). Acyl-CoAs were separated with an Acquity UPLC HSS T3 column (100 × 2 mm, 1.8 μm; Waters). The mobile phases A was 10 mM ammonium acetate (pH 6.8) and B was acetonitrile. The MS was operated in ESI^+ mode. Data were acquired using full scan over 800 to 1,200 *m/z* at 70,000 resolution.

Lipidomics. Total lipids were extracted using a previously reported method with minor modifications (80). Briefly, cell pellets were collected by centrifuging 10-mL culture aliquots and resuspended in 1.5 mL cold methanol. Then, 5 mL of methyl *tert*-butyl ether (MTBE) was added and the mixture was sonicated for 1 h. Phase separation was induced by adding 1.25 mL cold water followed by incubation at room temperature for 10 min. After centrifugation, lipid extracts were decanted, and cell pellets were subjected to an additional extraction using MTBE/methanol/water (10:3:2.5, vol/vol/vol). The extracts were pooled and dried under nitrogen gas.

To release fatty acids from lipids, saponification was performed by resuspending the dried lipids in 1 mL 90% methanol with 0.3 M KOH and incubating at 80 °C for 1 h. The samples were then neutralized with formic acid and extracted twice with hexane. The extracts were vacuum-dried, dissolved in pyridine, and derivatized at 80 °C for 30 min with *N*,*O*-bis [trimethylsilyl]trifluoroacetamide (with 1% trimethylchlorosilane; Sigma). The samples (1 μL) were injected into the GC-MS system described above.

The lipids were dissolved in acetonitrile/isopropanol/water (6:3:1, vol/vol/vol) to 1 $g{\cdot}L^{-1}$ and analyzed by an LC-30A UHPLC (Shimazu) coupled to a Q Exactive hybrid quadrupole-orbitrap MS (Thermo Fisher). The injection volume was 3 μL. Lipids were separated with an Acquity UPLC HSS C18 columm (100 × 2.1 mm, 1.7 μm; Waters). The mobile phase A was 10 mM ammonium formate and 0.1% formic acid in 60% water and 40% acetonitrile, and B was 10 mM ammonium formate and 0.1% formic acid in 90% isopropanol and 10% acetonitrile. The mass spectrometer was run in both ESI^+ and ESI^- modes. Lipid identification was performed with the LipidSearch (Thermo) and by querying the *m/z* in the mycobacteria-specific database MycoMass at a 5-ppm mass window with the TraceFinder software (81). The PGL was identified by matching *m/z* to the lipids from *M. marinum* (82). For each lipid class, individual molecular species that possess various alkane chain length or unsaturation degree were tracked by mass and their peak intensities were summed up to calculate the abundance of the lipid class.

Thin-layer chromatography (TLC) of the lipids was performed on silica gel 60-precoated plates F254 (Merck) (83). The lipids were developed with chloroform/methanol/water (20:4:0.5, vol/vol/vol). The TLC plate was sprayed with α-naphthol to specifically reveal glycolipids.

Quantification of Metabolic Fluxes. Mass isotopomer distributions (MIDs) of intact and fragmented metabolites were determined from measured peak areas of the mass spectra and corrected for naturally occurring stable isotopes as described previously (77). The fractional labeling of individual fatty acids was calculated from their MIDs (76). The fluxes or flux ratio, including the fatty acid-oxidation flux, malate from glyoxylate versus α-ketoglutarate, and the methylcitrate-cycle flux, was modeled with an individual small-scale ordinary differential equation system to simulate the dynamic labeling patterns of metabolites from the labeling patterns of their precursors (*SI Appendix*, Table S7). The model was then used to determine the fluxes or flux ratio by using the least-squares fitting of the simulated to the measured time-dependent MID of metabolites. All calculations were performed with MATLAB 7.8.0 (MathWorks).

Bioinformatics. Comparative genomic reconstruction of FdmR regulons in *Mycobacterium* species was performed using the RegPredict and GenomeExplorer tools based on identification of candidate regulator-binding sites in closely related prokaryotic genomes (84). For analysis of genetic variation of FdmR in clinical *M. tuberculosis* strains, the whole-genome sequences of 10,220 isolates were used (66). The ratio of nonsynonymous and synonymous substitutions (pNpS) of FdmR was calculated as described previously (85).

Statistics. Unless noted otherwise, data are presented as the mean ± SD of *n* independent experiments, and *P* values were calculated with two-tailed Student's *t* test. False discovery rate correction was performed using the two-stage step-up method of Benjamini, Krieger, and Yekutieli (86). The flux 95% confidence interval was determined on the basis of Monte Carlo simulations as described previously (87).

Data Availability. All the data generated or analyzed during this study are available within the main article and *SI Appendix*. RNA-Seq data have been deposited in the NCBI Sequence Read Archive under accession no. PRJNA657493 (88). ChIP-Seq data have been deposited in the Gene Expression Omnibus databank with accession code GSE156432 (89).

ACKNOWLEDGMENTS. We thank W. Hu and X. Xu for technical assistance on gas chromatography–quadrupole time-of-flight mass spectrometry. This work was supported by the National Natural Science Foundation of China (31830002 to G.-P.Z., 31925001 and 31921006 to C.Y., and 81991532 and 31970032 to L.-D.L.), the Chinese Academy of Sciences (XDB27020201 to C.Y.), the National Key R&D Program of China (2016YFC1303303 to C.Y. and 2018YFA0903700 to H.Z.), and the National Science and Technology Major Program of China (2018ZX10302301 to L.-D.L.).

1. H. Bloch, W. Segal, Biochemical differentiation of *Mycobacterium tuberculosis* grown *in vivo* and *in vitro*. *J. Bacteriol.* **72**, 132–141 (1956).
2. J. D. McKinney *et al*., Persistence of *Mycobacterium tuberculosis* in macrophages and mice requires the glyoxylate shunt enzyme isocitrate lyase. *Nature* **406**, 735–738 (2000).
3. J. Marrero, K. Y. Rhee, D. Schnappinger, K. Pethe, S. Ehrt, Gluconeogenic carbon flow of tricarboxylic acid cycle intermediates is critical for *Mycobacterium tuberculosis* to establish and maintain infection. *Proc. Natl. Acad. Sci. U.S.A.* **107**, 9819–9824 (2010).
4. J. Daniel, H. Maamar, C. Deb, T. D. Sirakova, P. E. Kolattukudy, *Mycobacterium tuberculosis* uses host triacylglycerol to accumulate lipid droplets and acquires a dormancy-like phenotype in lipid-loaded macrophages. *PLoS Pathog.* **7**, e1002093 (2011).
5. A. K. Pandey, C. M. Sassetti, Mycobacterial persistence requires the utilization of host cholesterol. *Proc. Natl. Acad. Sci. U.S.A.* **105**, 4376–4380 (2008).
6. C. Barisch, T. Soldati, *Mycobacterium marinum* degrades both triacylglycerols and phospholipids from its *Dictyostelium* host to synthesise its own triacylglycerols and generate lipid inclusions. *PLoS Pathog.* **13**, e1006095 (2017).
7. C. Barisch, T. Soldati, Breaking fat! How mycobacteria and other intracellular pathogens manipulate host lipid droplets. *Biochimie* **141**, 54–61 (2017).
8. C. M. Sassetti, E. J. Rubin, Genetic requirements for mycobacterial survival during infection. *Proc. Natl. Acad. Sci. U.S.A.* **100**, 12989–12994 (2003).
9. S. Ehrt, K. Rhee, D. Schnappinger, Mycobacterial genes essential for the pathogen's survival in the host. *Immunol. Rev.* **264**, 319–326 (2015).
10. K. Y. Rhee *et al*., Central carbon metabolism in *Mycobacterium tuberculosis*: An unexpected frontier. *Trends Microbiol.* **19**, 307–314 (2011).
11. S. Ehrt, K. Rhee, "*Mycobacterium tuberculosis* metabolism and host interaction: Mysteries and paradoxes" in *Pathogenesis of Mycobacterium tuberculosis and Its Interaction with the Host Organism*, J. Pieters, J. D. McKinney, Eds. (Springer, 2013), pp. 163–188.
12. J. Tong *et al*., The FBPase encoding gene *glpX* is required for gluconeogenesis, bacterial proliferation and division *in vivo* of *Mycobacterium marinum*. *PLoS One* **11**, e0156663 (2016).
13. R. R. Lovewell, C. M. Sassetti, B. C. VanderVen, Chewing the fat: Lipid metabolism and homeostasis during *M. tuberculosis* infection. *Curr. Opin. Microbiol.* **29**, 30–36 (2016).
14. G. Gago, L. Diacovich, H. Gramajo, Lipid metabolism and its implication in mycobacteria-host interaction. *Curr. Opin. Microbiol.* **41**, 36–42 (2018).
15. T. A. Gould, H. van de Langemheen, E. J. Muñoz-Elías, J. D. McKinney, J. C. Sacchettini, Dual role of isocitrate lyase 1 in the glyoxylate and methylcitrate cycles in *Mycobacterium tuberculosis*. *Mol. Microbiol.* **61**, 940–947 (2006).
16. J. E. Griffin *et al*., Cholesterol catabolism by *Mycobacterium tuberculosis* requires transcriptional and metabolic adaptations. *Chem. Biol.* **19**, 218–227 (2012).
17. S. Savvi *et al*., Functional characterization of a vitamin B12-dependent methylmalonyl pathway in *Mycobacterium tuberculosis*: Implications for propionate metabolism during growth on fatty acids. *J. Bacteriol.* **190**, 3886–3895 (2008).
18. S. T. Cole *et al*., Deciphering the biology of *Mycobacterium tuberculosis* from the complete genome sequence. *Nature* **393**, 537–544 (1998).
19. L. E. Quadri, Biosynthesis of mycobacterial lipids by polyketide synthases and beyond. *Crit. Rev. Biochem. Mol. Biol.* **49**, 179–211 (2014).
20. H. Marrakchi, M. A. Lanéelle, M. Daffé, Mycolic acids: Structures, biosynthesis, and beyond. *Chem. Biol.* **21**, 67–85 (2014).
21. J. E. Cronan Jr, S. Subrahmanyam, FadR, transcriptional co-ordination of metabolic expediency. *Mol. Microbiol.* **29**, 937–943 (1998).
22. Y. Fujita, H. Matsuoka, K. Hirooka, Regulation of fatty acid metabolism in bacteria. *Mol. Microbiol.* **66**, 829–839 (2007).
23. Y. T. Tsai, V. Salzman, M. Cabruja, G. Gago, H. Gramajo, Role of long-chain acyl-CoAs in the regulation of mycolic acid biosynthesis in mycobacteria. *Open Biol.* **7**, 170087 (2017).
24. R. K. Biswas *et al*., Identification and characterization of Rv0494: A fatty acid-responsive protein of the GntR/FadR family from *Mycobacterium tuberculosis*. *Microbiology (Reading)* **159**, 913–923 (2013).
25. S. Mondino, G. Gago, H. Gramajo, Transcriptional regulation of fatty acid biosynthesis in mycobacteria. *Mol. Microbiol.* **89**, 372–387 (2013).
26. J. E. Galagan *et al*., The *Mycobacterium tuberculosis* regulatory network and hypoxia. *Nature* **499**, 178–183 (2013).
27. S. L. Kendall *et al*., A highly conserved transcriptional repressor controls a large regulon involved in lipid degradation in *Mycobacterium smegmatis* and *Mycobacterium tuberculosis*. *Mol. Microbiol.* **65**, 684–699 (2007).
28. H. D. Park *et al*., Rv3133c/*dosR* is a transcription factor that mediates the hypoxic response of *Mycobacterium tuberculosis*. *Mol. Microbiol.* **48**, 833–843 (2003).

29. S. Ehrt, D. Schnappinger, K. Y. Rhee, Metabolic principles of persistence and pathogenicity in *Mycobacterium tuberculosis*. *Nat. Rev. Microbiol.* **16**, 496–507 (2018).
30. A. Aubry, F. Mougari, F. Reibel, E. Cambau, Mycobacterium marinum. *Microbiol. Spectr.* **5**, 10.1128/microbiolspec.TNMI7-0038-2016 (2017).
31. K. Takaki, J. M. Davis, K. Winglee, L. Ramakrishnan, Evaluation of the pathogenesis and treatment of *Mycobacterium marinum* infection in zebrafish. *Nat. Protoc.* **8**, 1114–1124 (2013).
32. T. C. Pozos, L. Ramakrishnan, New models for the study of *Mycobacterium*-host interactions. *Curr. Opin. Immunol.* **16**, 499–505 (2004). Correction in: *Curr. Opin. Immunol.* **17**, 95 (2005).
33. D. M. Tobin, L. Ramakrishnan, Comparative pathogenesis of *Mycobacterium marinum* and *Mycobacterium tuberculosis*. *Cell. Microbiol.* **10**, 1027–1039 (2008).
34. C. M. Sassetti, D. H. Boyd, E. J. Rubin, Genes required for mycobacterial growth defined by high density mutagenesis. *Mol. Microbiol.* **48**, 77–84 (2003).
35. Y. J. Zhang *et al*., Tryptophan biosynthesis protects mycobacteria from CD4 T-cell-mediated killing. *Cell* **155**, 1296–1308 (2013).
36. M. M. Bellerose *et al*., Distinct bacterial pathways influence the efficacy of antibiotics against *Mycobacterium tuberculosis*. *mSystems* **5**, e00396-20 (2020).
37. D. M. Langenau, L. I. Zon, The zebrafish: A new model of T-cell and thymic development. *Nat. Rev. Immunol.* **5**, 307–317 (2005).
38. S. Turkarslan *et al*., A comprehensive map of genome-wide gene regulation in *Mycobacterium tuberculosis*. *Sci. Data* **2**, 150010 (2015).
39. B. A. Covert, J. S. Spencer, I. M. Orme, J. T. Belisle, The application of proteomics in defining the T cell antigens of *Mycobacterium tuberculosis*. *Proteomics* **1**, 574–586 (2001).
40. J. E. Griffin *et al*., High-resolution phenotypic profiling defines genes essential for mycobacterial growth and cholesterol catabolism. *PLoS Pathog.* **7**, e1002251 (2011).
41. X. Chen *et al*., Structural basis for the broad substrate specificity of two acyl-CoA dehydrogenases FadE5 from mycobacteria. *Proc. Natl. Acad. Sci. U.S.A.* **117**, 16324–16332 (2020).
42. E. J. Muñoz-Elías, J. D. McKinney, *Mycobacterium tuberculosis* isocitrate lyases 1 and 2 are jointly required for *in vivo* growth and virulence. *Nat. Med.* **11**, 638–644 (2005).
43. C. B. Di Capua, M. Doprado, J. M. Belardinelli, H. R. Morbidoni, Complete auxotrophy for unsaturated fatty acids requires deletion of two sets of genes in *Mycobacterium smegmatis*. *Mol. Microbiol.* **106**, 93–108 (2017).
44. D. R. Banerjee, R. Biswas, A. K. Das, A. Basak, Design, synthesis and characterization of dual inhibitors against new targets FabG4 and HtdX of *Mycobacterium tuberculosis*. *Eur. J. Med. Chem.* **100**, 223–234 (2015).
45. M. Cabruja, B. B. Lyonnet, G. Millán, H. Gramajo, G. Gago, Analysis of coenzyme A activated compounds in actinomycetes. *Appl. Microbiol. Biotechnol.* **100**, 7239–7248 (2016).
46. J. Lara *et al*., *Mycobacterium tuberculosis* FasR senses long fatty acyl-CoA through a tunnel and a hydrophobic transmission spine. *Nat. Commun.* **11**, 3703 (2020).
47. H. Link, K. Kochanowski, U. Sauer, Systematic identification of allosteric protein-metabolite interactions that control enzyme activity *in vivo*. *Nat. Biotechnol.* **31**, 357–361 (2013).
48. S. Puckett *et al*., Glyoxylate detoxification is an essential function of malate synthase required for carbon assimilation in *Mycobacterium tuberculosis*. *Proc. Natl. Acad. Sci. U.S.A.* **114**, E2225–E2232 (2017).
49. H. Eoh, K. Y. Rhee, Methylcitrate cycle defines the bactericidal essentiality of isocitrate lyase for survival of *Mycobacterium tuberculosis* on fatty acids. *Proc. Natl. Acad. Sci. U.S.A.* **111**, 4976–4981 (2014).
50. N. M. Wolf, H. J. Gutka, F. Movahedzadeh, C. Abad-Zapatero, Structures of the *Mycobacterium tuberculosis* GlpX protein (class II fructose-1,6-bisphosphatase): Implications for the active oligomeric state, catalytic mechanism and citrate inhibition. *Acta Crystallogr. D Struct. Biol.* **74**, 321–331 (2018).
51. N. Ruecker *et al*., Fumarase deficiency causes protein and metabolite succination and intoxicates *Mycobacterium tuberculosis*. *Cell Chem. Biol.* **24**, 306–315 (2017).
52. W. Lee, B. C. VanderVen, R. J. Fahey, D. G. Russell, Intracellular *Mycobacterium tuberculosis* exploits host-derived fatty acids to limit metabolic stress. *J. Biol. Chem.* **288**, 6788–6800 (2013).
53. C. Maksymiuk, A. Balakrishnan, R. Bryk, K. Y. Rhee, C. F. Nathan, E1 of α-ketoglutarate dehydrogenase defends *Mycobacterium tuberculosis* against glutamate anaplerosis and nitroxidative stress. *Proc. Natl. Acad. Sci. U.S.A.* **112**, E5834–E5843 (2015).
54. C. Trujillo *et al*., Triosephosphate isomerase is dispensable *in vitro* yet essential for *Mycobacterium tuberculosis* to establish infection. *mBio* **5**, e00085 (2014).
55. H. Eoh, K. Y. Rhee, Multifunctional essentiality of succinate metabolism in adaptation to hypoxia in *Mycobacterium tuberculosis*. *Proc. Natl. Acad. Sci. U.S.A.* **110**, 6554–6559 (2013).
56. M. B. Reed *et al*., A glycolipid of hypervirulent tuberculosis strains that inhibits the innate immune response. *Nature* **431**, 84–87 (2004).
57. M. Jackson, The mycobacterial cell envelope-lipids. *Cold Spring Harb. Perspect. Med.* **4**, a021105 (2014).
58. R. K. Maurya, S. Bharti, M. Y. Krishnan, Triacylglycerols: Fuelling the hibernating *Mycobacterium tuberculosis*. *Front. Cell. Infect. Microbiol.* **8**, 450 (2019).
59. L. Guenin-Macé, R. Siméone, C. Demangel, Lipids of pathogenic mycobacteria: Contributions to virulence and host immune suppression. *Transbound. Emerg. Dis.* **56**, 255–268 (2009).
60. E. Schweizer, J. Hofmann, Microbial type I fatty acid synthases (FAS): Major players in a network of cellular FAS systems. *Microbiol. Mol. Biol. Rev.* **68**, 501–517 (2004).
61. P. E. Kolattukudy, N. D. Fernandes, A. K. Azad, A. M. Fitzmaurice, T. D. Sirakova, Biochemistry and molecular genetics of cell-wall lipid biosynthesis in mycobacteria. *Mol. Microbiol.* **24**, 263–270 (1997).
62. C. Vilchèze *et al*., Phosphorylation of KasB regulates virulence and acid-fastness in *Mycobacterium tuberculosis*. *PLoS Pathog.* **10**, e1004115 (2014).
63. A. Bhatt, V. Molle, G. S. Besra, W. R. Jacobs Jr, L. Kremer, The *Mycobacterium tuberculosis* FAS-II condensing enzymes: Their role in mycolic acid biosynthesis, acid-fastness, pathogenesis and in future drug development. *Mol. Microbiol.* **64**, 1442–1454 (2007).
64. E. Tortoli, Microbiological features and clinical relevance of new species of the genus *Mycobacterium*. *Clin. Microbiol. Rev.* **27**, 727–752 (2014).
65. D. Pisu, L. Huang, J. K. Grenier, D. G. Russell, Dual RNA-Seq of Mtb-infected macrophages *in vivo* reveals ontologically distinct host-pathogen interactions. *Cell Rep.* **30**, 335–350.e4 (2020).
66. C. Allix-Béguec *et al*.; CRyPTIC Consortium and the 100,000 Genomes Project, Prediction of susceptibility to first-line tuberculosis drugs by DNA sequencing. *N. Engl. J. Med.* **379**, 1403–1415 (2018).
67. I. Comas *et al*., Human T cell epitopes of *Mycobacterium tuberculosis* are evolutionarily hyperconserved. *Nat. Genet.* **42**, 498–503 (2010).
68. B. W. Allen, "Mycobacteria. General culture methodology and safety considerations" in *Mycobacteria Protocols*, T. Parish, N. G. Stoker, Eds. (Humana Press, 1998), pp. 15–30.
69. Q. Wang *et al*., CpsA, a LytR-CpsA-Psr family protein in *Mycobacterium marinum*, is required for cell wall integrity and virulence. *Infect. Immun.* **83**, 2844–2854 (2015).
70. L. Rodrigues, M. Viveiros, J. A. Aínsa, "Measuring efflux and permeability in mycobacteria" in *Mycobacteria Protocols*, T. Parish, D. M. Roberts, Eds. (Springer, 2015), pp. 227–239.
71. Z. Chen *et al*., Mycobacterial WhiB6 differentially regulates ESX-1 and the Dos regulon to modulate granuloma formation and virulence in zebrafish. *Cell Rep.* **16**, 2512–2524 (2016).
72. M. D. Robinson, D. J. McCarthy, G. K. Smyth, edgeR: A Bioconductor package for differential expression analysis of digital gene expression data. *Bioinformatics* **26**, 139–140 (2010).
73. C. K. Stover *et al*., New use of BCG for recombinant vaccines. *Nature* **351**, 456–460 (1991).
74. Y. Zhang *et al*., Model-based analysis of ChIP-seq (MACS). *Genome Biol.* **9**, R137 (2008).
75. T. L. Bailey, N. Williams, C. Misleh, W. W. Li, MEME: Discovering and analyzing DNA and protein sequence motifs. *Nucleic Acids Res.* **34**, W369–W373 (2006).
76. A. Nanchen, T. Fuhrer, U. Sauer, "Determination of metabolic flux ratios from 13C-experiments and gas chromatography-mass spectrometry data" in *Metabolomics: Methods and Protocols*, W. Weckwerth, Ed. (Humana Press, 2007), pp. 177–197.
77. J. Yuan, B. D. Bennett, J. D. Rabinowitz, Kinetic flux profiling for quantitation of cellular metabolic fluxes. *Nat. Protoc.* **3**, 1328–1340 (2008).
78. H. Zhang *et al*., The cyanobacterial ornithine-ammonia cycle involves an arginine dihydrolase. *Nat. Chem. Biol.* **14**, 575–581 (2018).
79. X. Yang, Y. Ma, N. Li, H. Cai, M. G. Bartlett, Development of a method for the determination of acyl-CoA compounds by liquid chromatography mass spectrometry to probe the metabolism of fatty acids. *Anal. Chem.* **89**, 813–821 (2017).
80. V. Matyash, G. Liebisch, T. V. Kurzchalia, A. Shevchenko, D. Schwudke, Lipid extraction by methyl-tert-butyl ether for high-throughput lipidomics. *J. Lipid Res.* **49**, 1137–1146 (2008).
81. E. Layre *et al*., A comparative lipidomics platform for chemotaxonomic analysis of *Mycobacterium tuberculosis*. *Chem. Biol.* **18**, 1537–1549 (2011).
82. S. S. Chavadi *et al*., Inactivation of *tesA* reduces cell wall lipid production and increases drug susceptibility in mycobacteria. *J. Biol. Chem.* **286**, 24616–24625 (2011).
83. A. E. Grzegorzewicz *et al*., Inhibition of mycolic acid transport across the *Mycobacterium tuberculosis* plasma membrane. *Nat. Chem. Biol.* **8**, 334–341 (2012).
84. D. A. Rodionov, Comparative genomic reconstruction of transcriptional regulatory networks in bacteria. *Chem. Rev.* **107**, 3467–3497 (2007).
85. A. Trauner *et al*., The within-host population dynamics of *Mycobacterium tuberculosis* vary with treatment efficacy. *Genome Biol.* **18**, 71 (2017).
86. Y. Benjamini, A. M. Krieger, D. Yekutieli, Adaptive linear step-up procedures that control the false discovery rate. *Biometrika* **93**, 491–507 (2006).
87. M. Hörl, J. Schnidder, U. Sauer, N. Zamboni, Non-stationary (13)C-metabolic flux ratio analysis. *Biotechnol. Bioeng.* **110**, 3164–3176 (2013).
88. W. Dong, Mycobacterial fatty acid catabolism is repressed by FdmR to sustain lipogenesis and virulence. Sequence Read Archive (SRA). https://www.ncbi.nlm.nih.gov/bioproject/PRJNA657493. Deposited 17 August 2020.
89. W. Dong, Mycobacterial fatty acid catabolism is repressed by FdmR to sustain lipogenesis and virulence. *Gene Expression Omnibus* (GEO). https://www.ncbi.nlm.nih.gov/geo/query/acc.cgi?acc=GSE156432. Deposited 18 August 2020.